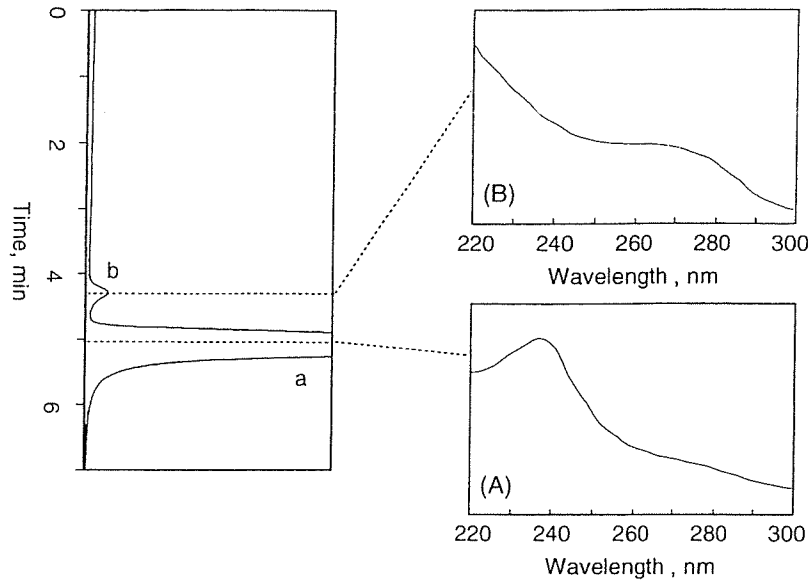

Fig. 3. The results detected by photodiode-array for unknown degradation product (b) and intact nicardipine (a).

3.3. Appearance change in polymorphs of nicardipine hydrochloride

Fig. 4 shows the time courses for discoloration of nicardipine hydrochloride under the white fluorescent lamp at 25 °C and 0%RH. The surface color of all tablets prepared from the two crystalline forms and the ground samples turned gradually from light yellow to orange-yellow upon exposure to light. The color change of all tablets became more intense with increasing irradiation time. The tablets of α-form ground samples were easy to discolor as compared with tablets of the crystals, whereas the ΔE value of β-form was greater than α-form after 13-d irradiation. As we have already reported on the discoloration of nifedipine tablet (Teraoka et al., 1999), the surface of nifedipine tablet also turned gradually from fresh yellow to dark yellow upon exposure to light by mercury vapor and fluorescent lamps. This suggests that such 1,4-dihydropyridine derivatives are susceptible to photodegradation. There are few reports with respect to photostability of modifications. Matsuda and Tatsumi (1990) reported that distinctly different degree of physicochemical photostability (coloration) was evident among the modifications of furosemide and the stable form did not show significant coloration even when irradiated with intense light. The solid-state photolytic degradation of two polymorphic forms of furosemide was investigated by De Villiers et al. (1992). Form I was photochemically more stable than form II, especially under a nitrogen atmosphere.

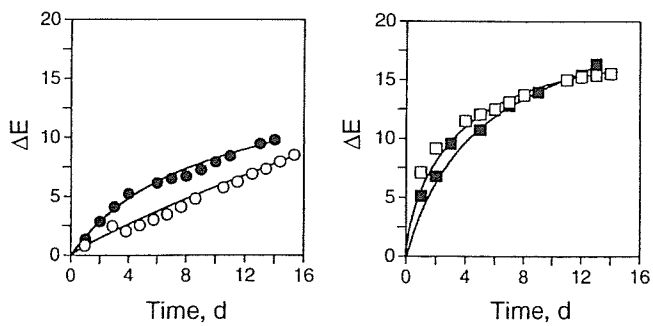

Fig. 4. Changes in color difference (ΔE) of α- (○,●) and β- (□,■) forms of nicardipine hydrochloride before and after grinding. The open and closed symbols represent the intact and ground powder after 150 min, respectively.

The surface of carbamazepine pellets turned gradually from white to yellow-orange upon exposure to light for all crystalline forms, and the discoloration rate of form II was faster than that of forms I and III (Matsuda et al., 1994).

3.4. Evaluation of photodegradation on the surface of nicardipine hydrochloride tablets

Fig. 5 shows the FT-IR-RAS spectra of β-form of nicardipine hydrochloride tablet before and after irradiation for 14 d under the white fluorescent lamp. The absorption peak at 1700 cm^{-1} attributable to the

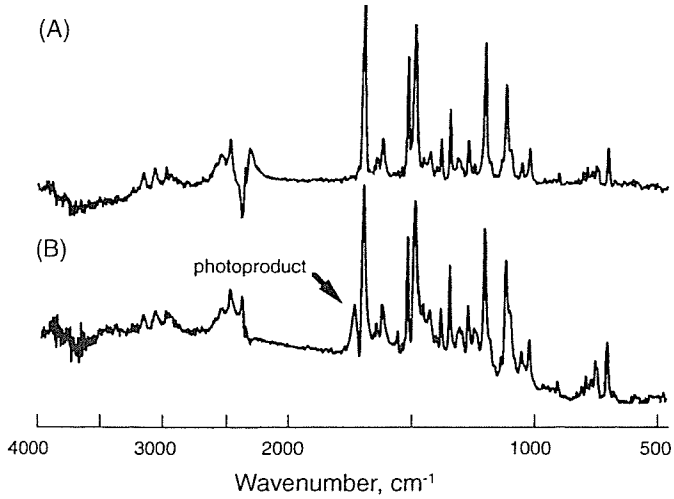

Fig. 5. Changes in FT-IR-RAS spectra of β-form of nicardipine hydrochloride before and after irradiation: (A) before irradiation; (B) after 14-d irradiation.

C=O stretch vibration of β-form decreased after irradiation and a new band appeared at 1734 cm^{-1}. The C=O stretch vibration band of pyridine derivative of nifedipine photoproducts was shifted to slightly higher wavenumber (Teraoka et al., 1999). In addition, the results obtained by a photodiode array detector showed that a pyridine derivative of nicardipine hydrochloride formed by light irradiation. The photodegradation of nicardipine hydrochloride solutions was investigated (Bonferoni, 1992) and the pyridine analog yielded after exposure to UV and daylight. This suggested that the residual nicardipine hydrochloride on the tablet surface decreased by photodegradation and a nitro-derivative formed.

The calibration curve for carbamazepine on the surface of pellet established good linearity and the reproducibility of the data was good (Matsuda et al., 1994). FT-IR-RAS method also allowed the separation of the intact nicardipine hydrochloride from the photoproducts in this study. Therefore, we used the absorbance of the C=O stretch band to measure the residual amount of the drug and the absorbance ratio of the C=O group at 1700 cm^{-1} before and after irradiation was calculated as the apparent residual nicardipine hydrochloride.

Fig. 6 shows the time-courses of the photodegradation of nicardipine hydrochloride tablets prepared with the two crystal forms and the ground samples under the irradiation by fluorescent lamp. The residual amount of the β-form ground decreased to approximately 10% after 12-d irradiation. On the other hand, about 40%

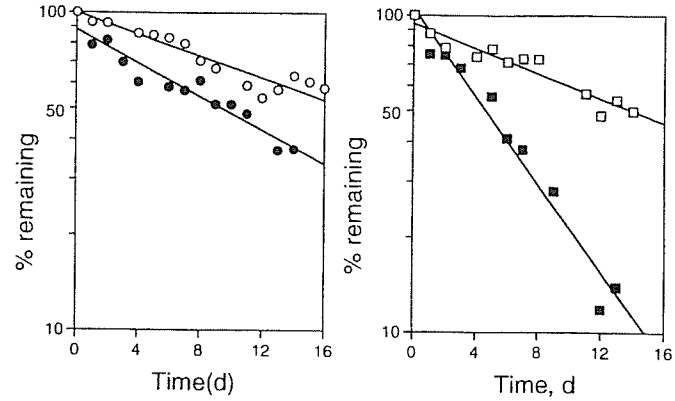

Fig. 6. Effect of grinding on the solid-state photostability of α- and β-forms of nicardipine hydrochloride (○,●): α-form; (□,■): β-form. The open and closed symbols represent the intact and ground powder after 150 min, respectively.

of intact amount remained in the case of the α-form ground after the same irradiation time. These results indicated that there was the significant difference in photostability between the ground sample of α-form and that of β-form.

Straight lines were obtained on the semilogarithmic scale for all tablets, indicating that photodegradation of the drug on the tablet surface followed apparently the first-order kinetics. Thus the degradation rate constants for these tablets were estimated from the linear part of the lines by least-squares method.

Table 1 summerizes photodegradation rate constants and the values of ΔE after 7-d irradiation for α- and β-forms. The values of ΔE of β-form and the ground sample exhibited approximately the same values, whereas the photodegradation rate constant for the β-ground sample was 3.5 times greater than that for β-form. Consequently, the appearance change was not in agreement with the degradation amount. This result suggested that it was difficult to estimate chemical stabil-

Table 1
Effect of grinding on the photodegradation rate constant and color difference (ΔE) after 7-d irradiation

	Degradation rate constant (d^{-1})	Color difference (ΔE) after 7-d irradiation
α-Form		
Intact	0.039	3.5
Ground for 150 min	0.061	6.5
β-Form		
Intact	0.046	13.1
Ground for 150 min	0.159	12.9

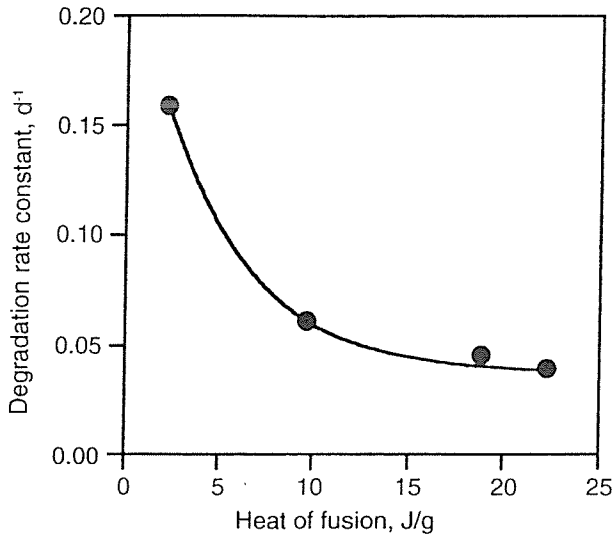

Fig. 7. Relationship between heat of fusion and photodegradation rate constant.

ity of nicardipine hydrochloride from the appearance change.

The photodegradation rate constants for β-form of lower melting point became greater than that for α-form. It has become apparent that β-form was less stable to light. The relation between the crystal structure of titanylphthalocyanine and its absorption spectrum in the solid state was investigated in detail (Mizuguchi et al., 1995). It was evident that the absorption spectrum in the solid state depends largely on the crystal form. Therefore, it would be thought that the two forms of nicardipine hydrochloride have its own absorption spectrum and the difference in photoreactivity was observed consequently among these crystal forms.

Both of the ground samples of two crystal forms decomposed much faster than each intact crystal and the ground sample of β-form was much more subject to photodegradation. It is considered that the ground sample had poor stability because the degree of crystallinity decreased by mechanochemical effect and due to the increase of internal energy. Fig. 7 illustrates the relationship between the photodegradation rate constant and heat of fusion measured by DSC profiles. The degradation rate constant decreased with increasing the heat of fusion. This suggested that the light stability depended on the crystal form and that the drug of the lower crystallinity was unstable both thermodynamically and photochemically.

4. Conclusion

It was proved that nicardipine hydrochloride in the solid state decomposed to a pyridine analog after oxidation of dihydropyridine ring by the light irradiation. Photodegradation of the ground crystals of the two forms was accelerated and this effect of grinding was especially significant for β-form crystals. The photostability of those powders decreased with the increase of internal energy of crystal.

FT-IR-RAS method is a simple and useful method for quantification of topochemical reaction such as solid-state photodegradation.

Acknowledgments

The authors are grateful to Yamanouchi Pharmaceutical Co., Ltd. for providing the two crystallines of nicardipine hydrochloride.

References

Akimoto, K., Kurosaka, K., Nakagawa, H., Sugimoto, I., 1988. A new approach to evaluating photo-stability of nifedipine and its derivatives in solution by actinometry. Chem. Pharm. Bull. 36, 1483–1490.

Augustyniak, W., Mielcarek, J., Milewski, M., Szamburska, O., 2001. Spectroscopic and HPLC studies of photodegradation of nilvadipine. Drug Dev. Ind. Pharm. 27, 1031–1038.

Baaske, D.M., DeMay, J.F., Latona, C.A., Mirmira, S., Sigvardson, K.W., 1996. Stability of nicardipine hydrochloride in intravenous solutions. Am. J. Health Syst. Pharm. 53, 1701–1705.

Binda, M.L., Dondi, G., 1981. Effect of light and coloring agents on the stability of nifedipine capsules. Boll. Chim. Farm. 120, 544–551.

Bonferoni, M.C., Mellerio, G., Giunchedi, P., Caramella, C., Conte, U., 1992. Photostability evaluation of nicardipine hydrochloride solutions. Int. J. Pharm. 80, 109–117.

De Filippis, P., Bovina, E., Da Ros, L., Fiori, J., Cavrini, V., 2002. Photodegradation studies on lacidipine in solution: basic experiments with a cis-trans reversible photoequilibrium under UV-A radiation exposure. J. Pharm. Biomed. Anal. 27, 803–812.

De Villiers, M.M., Van der Watt, J.G., Lotter, A.P., 1992. Kinetic study of the solid-state photolytic degradation of two polymorphic forms of furosemide. Int. J. Pharm. 88, 275–283.

Ebel, S., Schutz, H., Hornitschek, A., 1978. Analysis of nifedipine light degradation products. Arzneimittel-Forschung 28, 2188–2193.

Golden, W.G., 1985. In: Ferraro, J.R., Basile, L.J. (Eds.), Fourier Transform Infrared Spectroscopy. Academic Press, New York, p. 315.

Iwatani, M., Shibamura, T., Fujimoto, M., Kawai, R., Tamazawa, T., Takenaka, T., Takahashi, K., Murakami, M., 1979. Synthesis of new water-soluble dihydropyridine vasodilators. Chem. Pharm. Bull. 27, 1426–1440.

Kitamura, S., Miyamae, A., Koda, S., Morimoto, Y., 1989. Effect of grinding on the solid-state stability of cefixime trihydrate. Int. J. Pharm. 56, 125–134.

Matsuda, Y., Akazawa, R., Teraoka, R., Otsuka, M., 1994. Pharmaceutical evaluation of carbamazepine modifications: comparative study for photostability of carbamazepine polymorphs by using Fourier-transformed reflection-absorption infrared spectroscopy and colorimetric measurement. J. Pharm. Pharmacol. 46, 162–167.

Matsuda, Y., Tatsumi, E., 1990. Physicochemical characterization of furosemide modifications. Int. J. Pharm. 60, 11–26.

Matsuda, Y., Teraoka, R., Sugimoto, I., 1989. Comparative evaluation of photostability of solid-state nifedipine under ordinary and intensive light irradiation conditions. Int. J. Pharm. 54, 211–221.

Mielcarek, J., Stobiecki, M., Franski, R., 2000. Identification of photodegradation products of nilvadipine using GC-MS. J. Pharm. Biomed. Anal. 24, 71–79.

Mizuguchi, J., Rihs, G., Karfunkel, H.R., 1995. Solid-state spectra of titanylphthalocyanine as viewed from molecular distortion. J. Phys. Chem. 99, 16217–16227.

Qin, X., Frech, P., 2001. Liquid chromatography/mass spectrometry (LC/MS) identification of photooxidative degradates of crystalline and amorphous MK-912. J. Pharm. Sci. 90, 833–844.

Sturm, J.C., Nunez-Vergara, L.J., De la Fuente, J., Castro, C., Navarrete-Encina, P., Squella, J.A., 2001. Substituent effects on the electrochemistry and photostability of model compounds of calcium channel antagonist drugs. J. Electrochem. Soc. 148, E399–E404.

Teraoka, R., Otsuka, M., Matsuda, Y., 1999. Evaluation of photostability of solid-state dimethyl 1,4-dihydro-2,6-dimethyl-4-(2-nitro-phenyl)-3,5-pyridinedicarboxylate by using Fourier-transformed reflection-absorption infrared spectroscopy. Int. J. Pharm. 184, 35–43.

Thoma, K., Klimek, R., 1985. Untersuchungen zur Photoinstabilität von Nifedipin 1. Mitt. Zersetzungskinetik und Reaktionsmechanismus. Pharm. Ind. 47, 207–215.

Yan, J., Giunchedi, P., 1990. Characterization of a and b crystalline forms of nicardipine hydrochloride. Boll. Chim. Farmaceutico 129, 276–278.

Effect of Relative Humidity on the Photocatalytic Activity of Titanium Dioxide and Photostability of Famotidine

K. KAKINOKI,[1] K. YAMANE,[1] R. TERAOKA,[2] M. OTSUKA,[2] Y. MATSUDA[2]

[1]Manufacture Technology Department, Taiho Pharmaceutical Company, Ltd., 224-2, Ebisuno, Hiraishi, Kawauchi-cho, Tokushima 771-0194, Japan

[2]Department of Pharmaceutical Technology, Kobe Pharmaceutical University, 4-19-1, Motoyama-Kitamachi, Higashi-Nada, Kobe 658-8558, Japan

Received 19 January 2003; revised 1 May 2003; accepted 2 September 2003

Published online 17 December 2003 in Wiley InterScience (www.interscience.wiley.com). DOI 10.1002/jps.10575

ABSTRACT: Titanium dioxide (TiO_2) has been widely used as a pharmaceutical excipient and is also known to be a strong photocatalyst. An investigation into the relationship between the photocatalytic activity of TiO_2 and the photostability of famotidine, which is known as an H_2-blocker, is presented. The photocatalytic activity of the anatase form of TiO_2, as measured by the four-probe method, is ~1.5 times higher than that of the rutile form. Discoloration of famotidine in a binary system containing TiO_2 depends significantly on both the wavelength of the irradiating light and the crystal form of the TiO_2, with the degree of discoloration of anatase higher than that of the rutile form. Discoloration of famotidine also depends on relative humidity. The relationship between discoloration rate constant and water vapor pressure is linear. These results demonstrate that famotidine is easily discolored by the photocatalytic activity of TiO_2 and suggest that the solid-state photocatalytic activity of TiO_2 is strongly affected by relative humidity. © 2004 Wiley-Liss, Inc. and the American Pharmacists Association J Pharm Sci 93:582–589, 2004

Keywords: preformulation; physical stability; excipients; polymorph; materials science; TiO_2

INTRODUCTION

Titanium dioxide (TiO_2) has been known to be an effective inorganic pigment for a long time. Recently, TiO_2 has come to be widely used in many industries, including cosmetics, food additives, pharmaceuticals, and environment purification. In particular, over the last several decades, TiO_2 has been considered by many material scientists to be a strong photocatalyst.[1] In some studies about the photocatalysis of TiO_2, the solid-state photocatalytic activity of TiO_2 has been linked to oxidation–reduction reactions by some kind of moisture-derived radicals between the substrate and TiO_2. A possible mechanism for the formation of these radicals is the following series of reactions:[1–7]

$$TiO_2 + h\nu \rightarrow e^- + h^+ \quad (1)$$

$$e^- + O_2 \rightarrow \cdot O_2^- \quad (2)$$

$$h^+ + H_2O \rightarrow \cdot OH + H^+ \quad (3)$$

$$\cdot O_2^- + H^+ \leftrightarrow HO_2\cdot \quad (4)$$

In these chemical reactions, e^- and h^+ represent electrons and positive holes, respectively. Because of their photocatalytic properties, TiO_2 particles used as an inorganic white pigment instead of a catalyst are usually coated with hydroxylate metals to prevent generation and reaction of radicals by photocatalytic activity. However, coating

Correspondence to: Koichi Kakinoki (Telephone: 81 886 65 6054; Fax: 81 886 65 7995; E-mail: k-kakinoki@taiho.co.jp)

Journal of Pharmaceutical Sciences, Vol. 93, 582–589 (2004)

the surface of TiO_2 particles reduces the chemical purity, and the purity of TiO_2 for pharmaceutical use is strictly regulated. The Japanese Pharmacopoeia requires >98.5% purity, and the United States Pharmacopeia, requires >99.0% purity. As a result, the surfaces of TiO_2 particles for pharmaceutical use are not coated, and even if they were coated, the amount of hydroxylate metal would need to be very small. Thus, TiO_2 for pharmaceutical use is expected to exhibit photocatalytic activity. In spite of these facts, when TiO_2 is used in pharmaceutical products, no measures are taken in terms of protection from light and/or mutual reactions between drugs with which TiO_2 acts as a photocatalyst. Some drugs are often easily decomposed by light. So, evaluation of the photostability of these pharmaceutics is required to assure consistently high quality. Therefore, when TiO_2 is used in pharmaceutical formulations, the photocatalytic activity of TiO_2 and interactions between the drug and TiO_2 must be investigated.

Famotidine, which is known as an H_2-blocker, is stable under irradiation by light, but in the presence of TiO_2 was observed to undergo remarkable discoloration during preliminary studies. This discoloration appears to have been due to the photocatalytic activity of TiO_2, with famotidine decomposed and discolored by photocatalytic reactions involving TiO_2. An investigation into the relationship between the photocatalytic activity of TiO_2 and the photostability of famotidine was thus conducted.

EXPERIMENTAL

Materials

Two commercially available crystal forms of TiO_2 were used; they are the anatase form and the rutile form. Surfaces of the TiO_2 particles were not coated with any material to examine the effect of only TiO_2 on famotidine. The specific surface areas of the anatase and rutile forms were 14.6 and 7.8 m^2/g, respectively, as determined by gas adsorption measurements (Flowsorb II model 2300, Shimadzu Company). The anatase form was supplied by Toho Titanium Company, Ltd., and the rutile form was supplied by Showa Chemical Company, Ltd. The famotidine was obtained from Nippon Bulk Yakuhin Company, Ltd. All other chemicals and reagents were analytical grade.

Binary mixtures of famotidine and TiO_2 were prepared as compacts without coatings for light irradiation testing. Powder mixtures were used to increase the contact probability of famotidine and TiO_2 particles as much as possible to facilitate discoloration of the famotidine, because the photoreaction between TiO_2 and famotidine relies on solid contact. Compacts were prepared by physically mixing famotidine and TiO_2 in a bowl at a mass ratio of 4:1. Mixtures of 25 mg of mass were compressed into 10-mm diameter, 1-mm thick compacts under a compression force of 10 kN using an accurate compression/tension testing machine (Autograph model IS-5000, Shimadzu Company).

Measurement of the Photocatalytic Activity of TiO_2

Before investigating the effects of the addition of TiO_2 on discoloration of famotidine, a method for measuring the photocatalytic activity of TiO_2 different than previously reported methods was developed.[2–6] The existing methods tend to be concerned with the degradants of substances photocatalyzed by TiO_2 under limited conditions. Our approach is based on direct detection of the electrochemical reactions caused by the photocatalytic activity of TiO_2. The four-probe method was successfully applied to these reactions as a direct measurement method.

A schematic of the experimental setup of the four-probe method is shown in Figure 1. TiO_2 (1% w/v) was dispersed in a 0.1% w/v aqueous solution of sodium hydrogen carbonate. The two pairs of probes were placed in this solution, with one pair linked to a voltmeter and the other to a

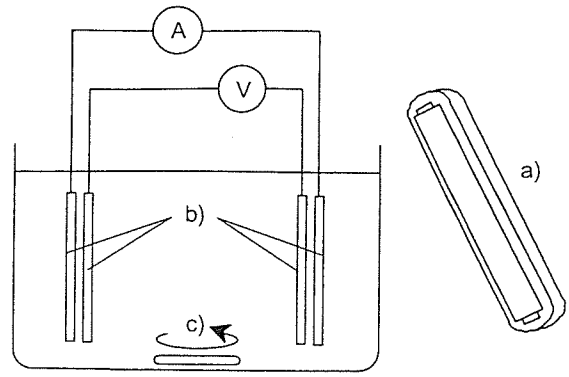

Figure 1. Experimental setup (four-probe method) for measuring photocatalytic activity of TiO_2. Key: (A) current source; (V) voltmeter, (a) near-UV lamp; (b) indium ingot probes; (c) stirring bar.

current source. The solution was stirred with a magnetic stirrer. The electric resistance of the solution was calculated by measuring the voltage at constant current.

As already described, radicals are produced by the photocatalytic activity of TiO_2. By irradiating the solution with a near-ultraviolet (UV) lamp (irradiation energy, 1.0 mW/cm^2), the electric resistance of the solution decreased as an increasing amount of radicals and ions were generated by photocatalytic activity of the TiO_2. This decrease in the electric resistance was thought to be due to the photocatalytic activity of TiO_2.

Measurement of Discoloration

Discoloration of the surfaces of samples was determined by measuring color differences (ΔE^*ab) using a chromameter (CR-221, Minolta Company, Ltd.) in the $L^*a^*b^*$ color system.

Irradiation Tests

Effect of Wavelength

Experiments were conducted at room temperature and ambient relative humidity (RH) with a monochromatic light source. Wavelengths were selected in the range 300–450 nm with a grating monochromator (CRM-50, JASCO Company), with the energy of monochromatic light incident on the sample set to 1.8×10^5 J/m^2. To set the same energy on the samples, the irradiation time was adjusted by the irradiation intensity for unit time defined by each wavelength.[8] After irradiation, color differences were calculated from surface color measurements performed on the sample compacts before and after irradiation.

Discoloration of Famotidine

Samples were placed in an environment of 30°C and 75% RH and irradiated by near-UV light (irradiation energy, 1.0 mW/cm^2). Changes in the colors of the samples as irradiation progressed were measured at several intervals. RH was maintained with a saturated aqueous solution of sodium chloride.

Effect of RH

Samples were placed in desiccators at 30, 60, 75, and 90% RH at 30°C and irradiated with near-UV light (irradiation energy, 1.0 mW/cm^2). Changes in the colors of the samples as irradiation progressed were measured at several intervals. RH was maintained with saturated aqueous solutions of several inorganic salts: 30% RH, magnesium dichloride hexahydrate; 60% RH, ammonium nitrate; 75% RH, sodium chloride; and 90% RH, potassium nitrate.

RESULTS

Measurement of Photocatalytic Activity

The changes in the electric resistance of an aqueous suspension of TiO_2 as measured by the four-probe method are shown in Figure 2. Significant reductions in relative resistance by light irradiation were observed for all types of TiO_2. Relative resistances were scaled to define electrical resistances under no irradiation as 100%. The relative resistance in the dispersed anatase system was confirmed to decrease by 40% after 20 min of irradiation, whereas in the rutile system, resistance decreased by 65%. These results suggest that the photocatalytic activity of the anatase form is ~1.5 times higher than that of the rutile form.

Irradiation Test

Effect of Wavelength

Famotidine was stable in light with no pharmaceutical excipient present, but discolored dramatically in the presence of TiO_2. The effect of wavelength on the discoloration of famotidine compacts is shown in Figure 3. The maximum color changes, which were easy to see with the

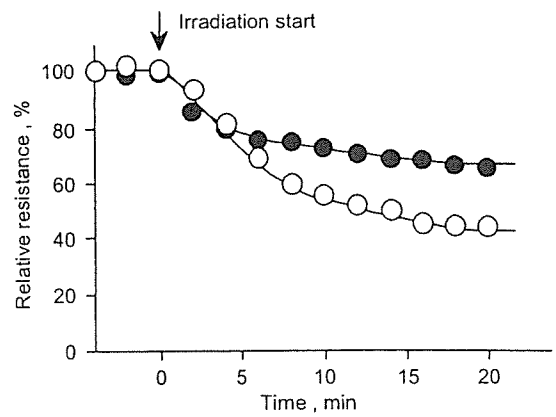

Figure 2. Photocatalytic activity of TiO_2 measured by the four-probe method. Key: (○) anatase form; (●) rutile form.

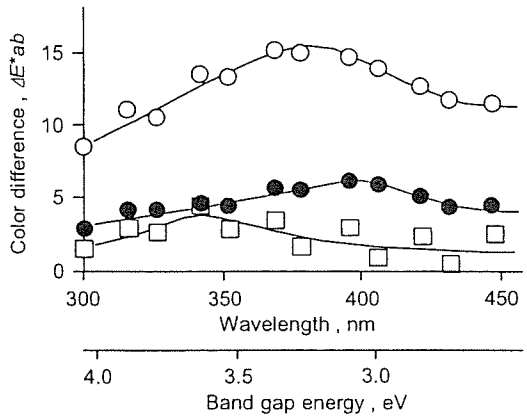

Figure 3. Effect of irradiating wavelength on the discoloration of famotidine compacts containing (○) the anatase form of TiO_2, (●) the rutile form of TiO_2, and (□) no TiO_2.

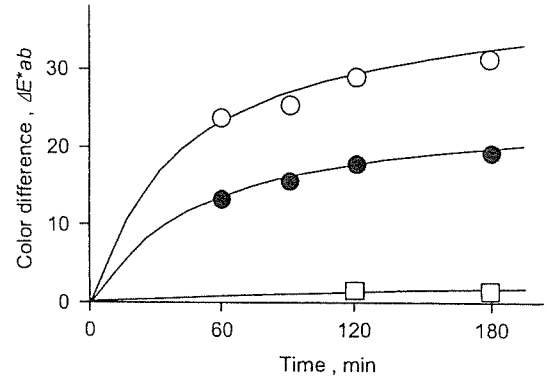

Figure 4. Effect of the photocatalytic activity of TiO_2 on the discoloration of famotidine at 30°C and 75% RH, for compacts containing (○) the anatase form of TiO_2, (●) the rutile form of TiO_2, and (□) no TiO_2.

naked eye, were produced by 380 nm light in the anatase system and by 400 nm light in the rutile system. Discoloration of famotidine without the presence of TiO_2 was also observed at ~340 nm. The extent of this color difference (ΔE^*ab) was quite small and could not be distinguished visually.[9]

Band gap energy (E) is the crystal-form-dependent energy needed for photocatalytic activity. The band gap energies of the anatase and rutile forms of TiO_2 are 3.2 and 3.0 eV, respectively,[1,10,11] and the relationship between band gap energy and wavelength of light is

$$E = h\upsilon = hc/\lambda \tag{5}$$

where h is Planck's constant, υ is the frequency of light, c is the velocity of light, and λ is the wavelength of light. Using eq. 5, the wavelength of light corresponding to the band gap energy of the anatase form was calculated as ~380 nm and that of the rutile form was calculated as ~410 nm. These wavelengths are in good agreement with the wavelengths inducing the maximum color changes in the famotidine compacts for each TiO_2 crystal form. This agreement of results suggests that the discoloration of famotidine in the presence of TiO_2 was induced by photocatalytic activity of TiO_2.

Discoloration of Famotidine

The effect of TiO_2 on the discoloration of famotidine compacts with time at 30°C and 75% RH is shown in Figure 4. Famotidine compacts containing no TiO_2 were slightly discolored after a long period of irradiation (3 h). In comparison, famotidine compacts containing TiO_2 in any crystal form were discolored quite significantly. Changes in the color of famotidine compacts containing the anatase form of TiO_2 were much greater than those in compacts containing the rutile form.

To kinetically interpret the discoloration of famotidine compacts containing TiO_2, the following equation, reported by Matsuda et al.,[12] was applied to the discoloration process:

$$d(\Delta E^*ab)/dt = k\,(\Delta E^*ab)^n \tag{6}$$

where t is the irradiation time, k is the discoloration rate constant, and n is the reaction order. Integrating eq. 6 gives

$$\ln(\Delta E^*ab) = 1/(1-n)\cdot\ln[(1-n)\cdot k] + 1/(1-n)\cdot\ln t \quad (n \neq 1) \tag{7}$$

If the discoloration of famotidine compacts follows eq. 7, the relationship between irradiation time and color change could be established by a double-logarithmic plot. Double-logarithmic plots of the anatase and rutile systems shown in Figure 4 are presented in Figure 5. A clear relationship between discoloration and time was confirmed to exist, with parallel lines for the anatase and rutile forms. This result suggests that the kinetic model of eq. 6 could be applied to the discoloration of famotidine compacts containing TiO_2.

Effect of RH

The photocatalytic activity of TiO_2 has generally been known to be influenced by RH.[13–17] The discoloration of famotidine compacts containing

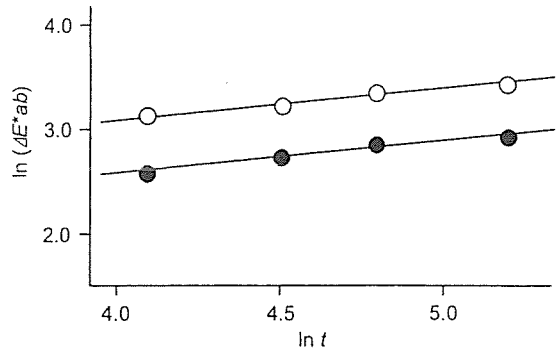

Figure 5. Double-logarithmic plots of the effect of photocatalytic activity of TiO_2 on the discoloration of famotidine compacts at 30°C and 75% RH, for compacts containing (○) the anatase form of TiO_2 and (●) the rutile form of TiO_2.

TiO_2 under various conditions of RH is plotted against time in Figure 6. The degree of color change increase significantly with increasing RH. On double-logarithmic plots of these discolorations, created with eq. 7, the slopes of lines calculated by the least squares method were 0.3–0.4 for the anatase form and 0.3–0.6 for the rutile form. The mechanisms of discoloration of famotidine compacts containing anatase and rutile forms are expected to be the same, because the photocatalysis by TiO_2 causes the same radical reactions, as already described. Thus, based on the same mechanism of radical reaction for both the anatase and rutile forms, all of the reaction orders are theoretically the same. Reaction orders were calculated from the slope of each line with eq. 7. A mean slope of 0.4 was obtained from the eight lines. Lines with a fixed slope of 0.4 fit the data well, showing good agreement with all of the results (see Fig. 7). The y-intercept was then calculated as the arithmetic mean for each RH. The discoloration rate constants calculated with eq. 7 at each RH are given in Table 1. The RH values were converted to water vapor pressures to allow interpretations to be made based on a water content parameter. Semi-logarithmic plots of the relationship between discoloration rate constant and water vapor pressure are shown in Figure 8. Good linear relationships were established between the logarithm of discoloration rate constant and water vapor pressure for each of the crystal forms, with a correlation coefficient of 0.996 for the anatase form and of 0.971 for the rutile form. The discoloration rate constant of the anatase system was larger than that of the rutile system at all water vapor pressures, indicating the higher photocatalytic activity of the anatase form. These results imply a relationship between discoloration rate constant and water vapor pressure of

$$\ln k = \ln k_0 + r \cdot P \qquad (8)$$

where P is water vapor pressure, r is a coefficient of relating water vapor pressure to discoloration rate constant, and k_0 is the discoloration rate constant at 0% RH. The values of r, calculated with eq. 8, are 3.55 for the anatase form and 5.57 for the rutile form. These results suggest that discoloration rate constant is significantly influenced by water vapor pressure in both crystal forms of TiO_2. Thus, the photocatalytic activity of TiO_2 is dependent on RH. The relationship between RH and the ratio of the discoloration rate

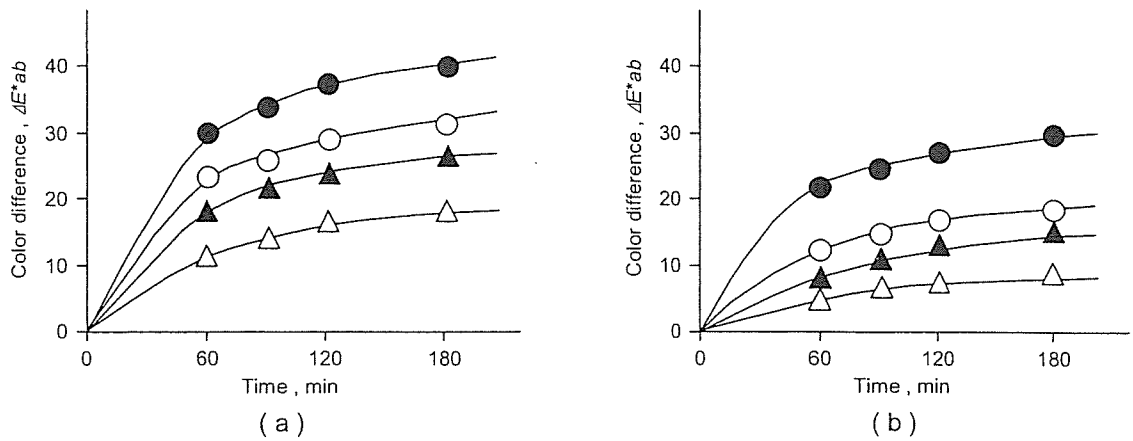

Figure 6. Effect of RH at 30°C on the discoloration of famotidine compacts containing (a) the anatase form of TiO_2 and (b) the rutile form of TiO_2. Key: (△) 30% RH; (▲) 60% RH; (○) 75% RH; and (●) 90% RH.

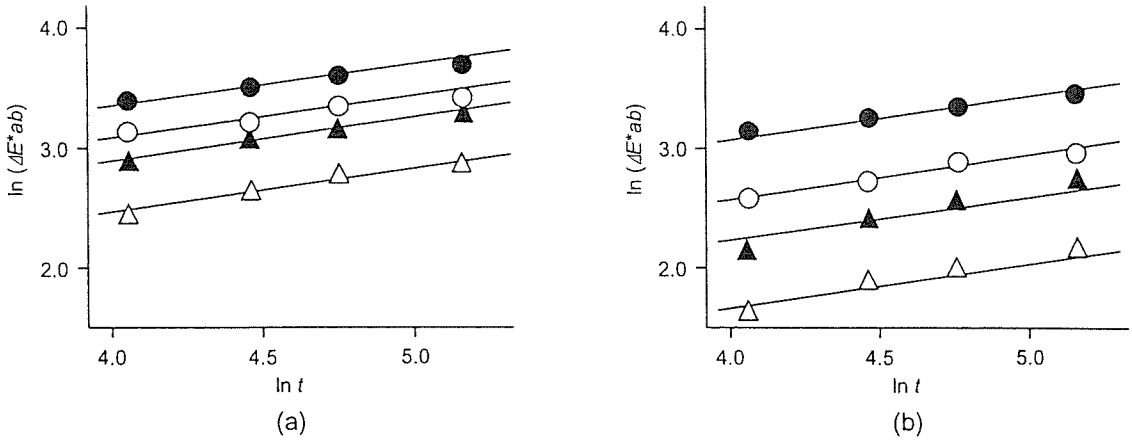

Figure 7. Regression lines with the same slope, as determined by double-logarithmic plots of the effect of RH at 30°C on the discoloration of famotidine compacts containing (a) the anatase form of TiO_2 and (b) the rutile form of TiO_2. Key: (△) 30% RH; (▲) 60% RH; (○) 75% RH; and (●) 90% RH.

constant of the anatase form to that of the rutile form is shown in Figure 9. The relationship is linear with a correlation coefficient of regression of 0.985. From the data in Figure 9, the ratio of the discoloration rate constant of the anatase form to that of the rutile form was estimated as ~1.5 at 100% RH. This result is in agreement with the ratio of the photocatalytic activity of anatase TiO_2 to that of rutile TiO_2 shown in Figure 2. The fact that the activity ratio at ~100% RH was almost equal to the ratio of photocatalytic activity of the anatase form to that of the rutile form in aqueous suspension verifies that the photocatalytic activity of TiO_2 is closely related to the photostability of famotidine compacts.

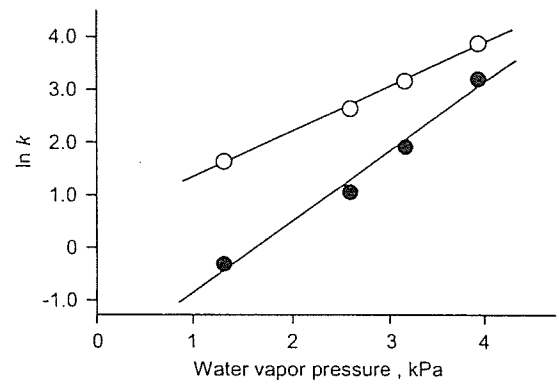

Figure 8. Semilogarithmic plots of the effect of water vapor pressure on discoloration rate constant for compacts containing (○) the anatase form of TiO_2 and (●) the rutile form of TiO_2.

DISCUSSION

The photocatalytic activity of anatase measured by the four-probe method was ~1.5 times higher than that of rutile. This result is in agreement with the ratio of the discoloration rate constant of

Table 1. k Values under Various Relative Humidity Conditions

Relative Humidity (%)	k (min^{-1})	
	Anatase System	Rutile System
30	5.0	0.8
60	14.1	2.9
75	23.3	6.4
90	46.4	24.9

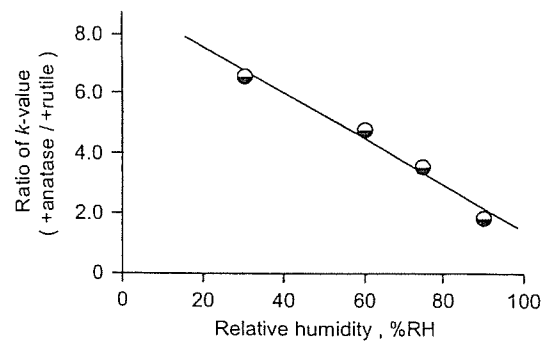

Figure 9. Relationship between the ratio of discoloration rate constants of anatase to rutile and RH ($y = -0.0762 \times +9.0804$; $r = 0.985$).

the anatase form to that of the rutile form at 100% RH. Differences in the degree of change in the appearance of famotidine compacts by adding TiO_2 are thus suggested to depend on differences in photocatalytic activity. Given this fact, the four-probe method has a possibility to be a benchmark technique for measuring the photocatalytic activity of TiO_2. Discoloration of famotidine compacts containing TiO_2 also depended on the wavelength of the irradiating light. Wavelengths corresponding to maximum discoloration correlated well with band gap energies for both TiO_2 crystal forms. This result suggests that discoloration was caused by solid-state reactions between famotidine and TiO_2 crystals. In addition, discoloration of famotidine compacts containing TiO_2 was enhanced by RH. Relationships between the RH and decomposition of drugs in the solid-state have been reported as very complex reaction models.[18–21] However, the relationship found between the discoloration rate constant of famotidine compacts containing TiO_2 and water vapor pressure could be clearly described by a simple power law. Thus, RH is a major factor affecting the photocatalytic activity of TiO_2 in solid-state photoreactions. Discoloration of famotidine in the presence of TiO_2 could be explained by several photocatalytic reaction models. Thus, the key factors in the reaction related to discoloration of the famotidine were the generation of radicals, as described earlier. On irradiation, e^- and h^+ are produced over the surface of TiO_2. However, the major cause of the reaction is thought to have been ·OH and/or HO_2· because these are more mobile. Thus, e^- and h^+ were continuously generated during the period of irradiation, but the probability of the production of ·OH and/or HO_2· depended on RH because RH determines the availability of the water molecules that are needed to generate ·OH and/or HO_2·. The reason the photocatalytic activity of the anatase form was more remarkable than that of the rutile form may be the ability to convert water molecule to radicals under low moisture conditions.

The main result of this study indicates that TiO_2 may decrease the photostability of drug because of its photocatalytic activity. The rutile form was shown to be preferable to the anatase form in improving the photostability of famotidine. In conclusion, to use TiO_2 as a pharmaceutical excipient, the photocatalytic activity of TiO_2 needs to be determined first. Furthermore, mutual interactions between TiO_2 and drugs need to be investigated in the preformulation stage.

ACKNOWLEDGMENTS

The authors are grateful to the staff of Ishikawajima-Harima Heavy Industries Company, Ltd. and Ishikawajima Inspection & Instrumentation Company, Ltd. for conducting the measurements of the photocatalytic activity of TiO_2.

REFERENCES

1. Fujishima A, Rao TN, Tryc DA. 2000. Titanium dioxide photocatalysis. J Photochem Photobiol C 1: 1–21.
2. Sabin F, Türk T, Vogler A. 1992. Photo-oxidation of organic compounds in the presence of titanium dioxide: determination of the efficiency. J Photochem Photobiol A 63:99–106.
3. Augugliaro V, Coluccia S, Loddo V, Marchese L, Martra G, Palmisano L, Schiavello M. 1999. Photocatalytic oxidation of gaseous toluene on anatase TiO_2 catalyst: Mechanistic aspects and FT-IR investigation. Appl Catal B 20:15–27.
4. Davydov L, Reddy EP, France P, Smirniotis PG. 2001. Sonophotocatalytic destruction of organic contaminants in aqueous systems on TiO_2 powders. Appl Catal B 32:95–105.
5. Khalyavka TA, Shimanovskaya VV, Strelko VV, Kapinus EI. 2001. Photocatalytic activity of titanium dioxide in the degradation of methylene blue and tetrachlorofluorescein in aqueous solutions. Theor Exp Chem 37:58–62.
6. Kang M, Lee SY, Chung CH, Cho SM, Han GY, Kim BW, Yoon KJ. 2001. Characterization of a TiO_2 photocatalyst synthesized by the solvothermal method and its catalytic performance for $CHCl_3$ decomposition. J Photochem Photobiol A 144:185–191.
7. Heredia JBD, Torregrosa J, Dominguez JR, Peres JA. 2001. Oxidation of *p*-hydroxybenzoic acid by UV radiation and by TiO_2/UV radiation: Comparison and modeling of reaction kinetic. J Hazard Mater B 83:255–264.
8. Matsuda Y, Teraoka R, Sugimoto I. 1989. Comparative evaluation of photostability of solid-state nifedipine under ordinary and intensive light irradiation conditions. Int J Pharm 54:211–221.
9. Matsuda Y, Minamida Y. 1976. Stability of solid dosage forms. I. Fading of several colored tablets by exaggerated light. Yakugaku Zasshi 96:425–433.
10. Tang H, Berger H, Schmid PE, Levy F, Burri G. 1993. Photoluminescence in TiO_2 anatase single crystals. Solid State Commun 87:847–850.
11. Pascual J, Camassel J, Mathieu H. 1978. Fine structure in the intrinsic absorption edge of titanium dioxide. Phys Rev B 18:5606–5614.

12. Matsuda Y, Masahara R. 1980. Comparative evaluation of discoloration of photosensitive solid drugs under various light sources. Yakugaku Zasshi 100:953–957.
13. Hoffmann E, Saracz A. 1969. Weathering of paint films. II. Chalking caused by anatase titanium dioxide in latex paints. J Oil Colour Chem Assoc 52:1130–1144.
14. Hoffmann E, Saracz A. 1972. Weathering of paint films. V. Chalking in emulsion paints films caused by silicone-coated anatase titanium dioxide and zinc oxide at varying humidities. J Oil Colour Chem Assoc 55:1079–1085.
15. Amama PB, Itoh K, Murabayashi M. 2001. Photocatalytic oxidation of trichloroethylene in humidified atmosphere. J Mol Catal A 176:165–172.
16. Wang KH, Hsieh YH, Lin CH, Chan CY. 1999. The study of the photocatalytic degradation kinetics for dichloroethylene in vapor phase. Chemosphere 39: 1371–1384.
17. Wang KH, Tsai HH, Hsieh YH. 1998. The kinetics of photocatalytic degradation of trichloroethylene in gas phase over TiO_2 supported on glass bead. Appl Catal B 17:313–320.
18. Teraoka R, Otsuka M, Matsuda Y. 1993. Effects of temperature and relative humidity on the solid-state chemical stability of ranitidine hydrochloride. J Pharm Sci 82:601–604.
19. Aruga M, Awazu S, Hanano M. 1978. Kinetic studies on decomposition of glutathione. I. Decomposition in solid state. Chem Pharm Bull 26:2081–2091.
20. Yoshioka S, Uchiyama M. 1986. Nonlinear estimation of kinetic parameters for solid-state hydrolysis of water-soluble drugs. J Pharm Sci 75:459–462.
21. Yoshioka S, Carstensen JT. 1990. Nonlinear estimation of kinetic parameters for solid-state hydrolysis of water-soluble drugs. II: Rational presentation mode below the critical moisture content. J Pharm Sci 79:799–801.

Effect of controlled zinc release on bone mineral density from injectable Zn-containing β-tricalcium phosphate suspension in zinc-deficient diseased rats

Makoto Otsuka,[1] Yuko Ohshita,[1] Sunao Marunaka,[1] Yoshihia Matsuda,[1] Atsuo Ito,[2] Noboru Ichinose,[3] Kuniko Otsuka,[4] William I. Higuchi[5]

[1]*Kobe Pharmaceutical University, Department of Pharmaceutical Technology, Motoyama-Kitamachi 4-19-1, Higashi-Nada, Kobe 658-8558, Japan*

[2]*National Institute of Advanced Industrial Science and Technology, Central 4, 1-1-1 Higashi Tsukuba, Ibaraki 305-8562, Japan*

[3]*Faculty of Science and Engineering, Okubo 3-4-1, Waseda University, Okubo, Shinjyuku, Tokyo, 169-8555, Japan*

[4]*School of Medicine, Showa University, Htanodai 1-5-8, Shinagawa, Tokyo 142-8555, Japan*

[5]*Department of Pharmaceutics and Pharmaceutical Chemistry, University of Utah, Salt Lake City, Utah 84112*

Received 24 May 2002; revised 2 February 2004; accepted 10 February 2004
Published online 6 April 2004 in Wiley InterScience (www.interscience.wiley.com). DOI: 10.1002/jbm.a.30040

Abstract: The purpose of this study was to evaluate the efficacy of zinc (Zn)-containing β-tricalcium phosphate (Zn–TCP) in correcting the bone mineral deficiency noted in osteoporosis using ovariectomized rat model. Four rats were used for each of the four experimental groups: D0, D10, D20, and N10. The rats in D0, D10, and D20 groups were ovariectomized, and fed a vitamin D-, Ca-, and Zn-deficient diet, and induced Zn-deficient osteoporoses for 9 weeks. In contrast, the N10 group was the normal rats fed normal healthy diet for 9 weeks. D0 group was injected with pure β-TCP suspension, D10 and D20 groups were injected with suspensions containing 10 mg of 10 mol % (6.17 wt % Zn) and 20 mol % (12.05 wt % Zn) Zn–TCP, respectively, and the healthy group, N10 were injected with 10 mol %. Zn–TCP suspensions. Injections were administered intramuscularly in the left thigh once a week in all rats, and fed a vitamin D- and Zn-deficient diet for 9 weeks. The plasma calcium (Ca) and Zn levels, plasma alkaline phosphatase activity (ALP) and bone mineral density (BMD) of the lumbar vertebra and femora were measured. The plasma Zn levels in all the rats were between 1.1 and 2.8 μg/mL. The areas under the curves for the Ca, Zn, and ALP (Ca-AUC, Zn-AUC, and ALP-AUC) levels between 0 and 63 days were calculated. Results for the AUCs were as follows: (1) the Zn-AUCs were in the order of N10 = D20 > D10 > D0; (2) the Ca-AUCs for D0, D10 groups were significantly lower than that for the N10 group; (3) the ALP-AUCs for the D10 and D20 groups were significantly higher than that for the N10 group, and that of the D0 group was in between those. The body weight of D10 and D20 groups significantly increased with time, that of the D0 group increased slightly, and that of the N10 group remained unchanged for the entire experimental period. The BMD of the lumbar vertebrae of the D10 and D20 groups (about 100 mg/cm^2) was significantly higher than that of the D0 group but lower than that of the N10 group. The BMD of the left femur increased more than that of the right femur with the increase in the amount of Zn in the suspension. The results of this study suggest that the local effect on BMD was more pronounced than the effect on the whole body. © 2004 Wiley Periodicals, Inc. J Biomed Mater Res 69A: 552–560, 2004

Key words: biomaterial; zinc; drug delivery system; tricalcium phosphate; *in vivo* release; bone mineral density; therapeutical improvement; zinc-deficient osteoporosis

INTRODUCTION

Zinc (Zn) is an essential trace element that is a cofactor of more than 200 enzymes and is present in nearly every cell type in the body.[1] It is important for immune system functioning, wound healing, and maintaining the senses of taste and smell. Zn inhibits the differentiation of osteoclasts,[2] and promotes osteoblast activity, thus affecting the formation of hard tissues. Therefore, Zn is biologically essential for maintaining good health in humans. Recently, a clinical relationship between osteoporosis and Zn deficiency has been established in elderly subjects.[3,4] However, although Zn may be useful for the treatment of osteoporosis, it was also reported that a high Zn concentration may have serious cytotoxic effects on cells.[1] Therefore, the range of Zn concentrations essen-

Correspondence to: M. Otsuka; e-mail: m-otsuka@kobepharma-u.ac.jp

Contract grant sponsor: the Science Research Promotion Fund of the Japan Private School Promotion Foundation
Contract grant sponsor: Japan Society for the Promotion of Sciences, and AIST (Agency of Industrial Science and Technology); contract grant number: KAKENHI 13680958

TABLE I
Vitamin D, Calcium, and Zinc Contents of Various Diets

Sample		Vit. D Content IU/100 g	Ca Content mg/100 g	Zn Content mg/100 g
-DCaZn	VD-, Ca-, and Zn-deficient diet	negative[a]	12[a]	0.08[a]
-DZn	VD- and Zn-deficient diet	negative	232	0.08
N	Normal diet	250[a]	1180[a]	6.38[a]

The rats were fed approximately 100 g of the diet per week.
[a]The data from Clea Co. Ltd., Osaka, Japan.

tial for an optimal biological response, that is, the therapeutic index, is narrow. Ito et al. applied tricalcium phosphate ceramics containing Zn (Zn–TCP) as a novel artificial bone material and demonstrated quantitatively that Zn–TCP stimulated bone formation around ceramic implants in rabbit femora.[5–7]

In addition, it has been demonstrated that the controlled release of antiosteoporosis drugs from apatite bone cement is effective for improving bone mineral density in osteoporotic rats.[8–10] Because Zn deficiency is a key factor for the induction of osteoporosis and other diseases, we developed an injectable Zn–TCP suspension to provide for a medical treatment of Zn deficiency diseases. The suspension formulation provides for the sustained release of Zn for more than 1 week. In the present study, we administered this suspension to Zn-deficient rats and assessed the Zn release behavior and its therapeutic effectiveness.

MATERIALS AND METHODS

Materials

Tricalcium phosphate powders [$Ca_3(PO_4)_2$, or TCP] containing 10 and 20 mol % Zn (6.17 and 12.05 w/w %) were synthesized and characterized using X-ray diffraction and scanning electron microscopy as described previously.[5,7] These materials were used for the new sustained release preparation. The nominal chemical formula of 10 mol % Zn–TCP was $Ca_{2.7}\ Zn_{0.3}\ (PO_4)_2$. Because the limit of zinc substitution for calcium in TCP is 12 mol %, the 20 mol % Zn–TCP is mixture of $Ca_{2.7}\ Zn_{0.3}\ (PO_4)_2$ and $Ca\ Zn_2\ (PO_4)_2$. SEM revealed that Zn–TCP powder samples consisted of aggregated particles. The individual particles were less than 1 μm in diameter, which was consistent with results published previously.[7]

Ca and Zn measurements

Ca concentration was determined based on the methylxyenol blue complex method[11] using a UV/VIS spectrometer (Type UV160, Shimadzu Co., Ind., Japan) at 610 nm. Zn concentration was determined at 213.8 nm by atomic absorption spectrometry (Type 180-70, Hitachi Co. Ind., Japan). All data are expressed as average values ± standard deviation of four different measured values. The area under the curves of plasma Zn and Ca levels (Zn-AUC and Ca-AUC) were calculated by integration of the plasma Zn and Ca level profiles as an useful parameter of the bioavailability of drug, respectively.

Diet for animals

A vitamin D-, Ca- and Zn-deficient (−DCaZn) diet was prepared and supplied by Clea Co. Ltd, Osaka, Japan. A normal (N) diet was obtained from Clea Co. Ltd. −DZn-diet was prepared by mixing calcium carbonate 1.38 g to 98.62 g of −DZnCa-diet as shown in Table I.

Animal study

Animal care was conducted according to the Animal Care Committee guidelines of Kobe Pharmaceutical University. The animals were anesthetized by ether inhalation during all surgery and injections. Figure 1 shows a flow diagram of the experimental protocol. Sixteen (16) female Wistar rats (from Crea Co. Japan), were assigned into four groups. The groups consisted of: the D0 group with induced osteoporosis and treated with pure TCP suspension injection: the D10 group with induced osteoporosis and treated with 10 mol % Zn–TCP suspension injection, and the D20 group with induced osteoporosis and treated with 20 mol % Zn–TCP suspension injection. The N10 group was healthy rats with treated by 10 mol % Zn–TCP suspension injection. Osteoporotic rats were prepared following the modified protocol, reported by Yamaguchi et al.[12] and Suda et al.[13] Ovariectomy was performed on rats in the D0, D10, and D20 groups, which were approximately 5 weeks old and had an average of weight 100 g. Following the surgery, the rats were fed the −DCaZn-diet for the first 9 weeks, and were induced Zn-deficient osteoporoses weighing 150–170 g, respectively, as shown in the lumber vertebra bone mineral densities below. On the other hand, the N10 group was fed the N-diet for the first 9 weeks. The Zn–TCP and TCP suspensions consisted of 10 mg of Zn–TCP or TCP powders, respectively, in 0.2 mL of physiological saline solution. After the first 9 weeks, injections of suspensions of Zn–TCP and TCP were initiated as shown in Figure 1. The Zn–TCP and TCP suspensions were injected intramuscularly in the left thigh of the rats in all groups once every 7 days, and repeated for a total of 10

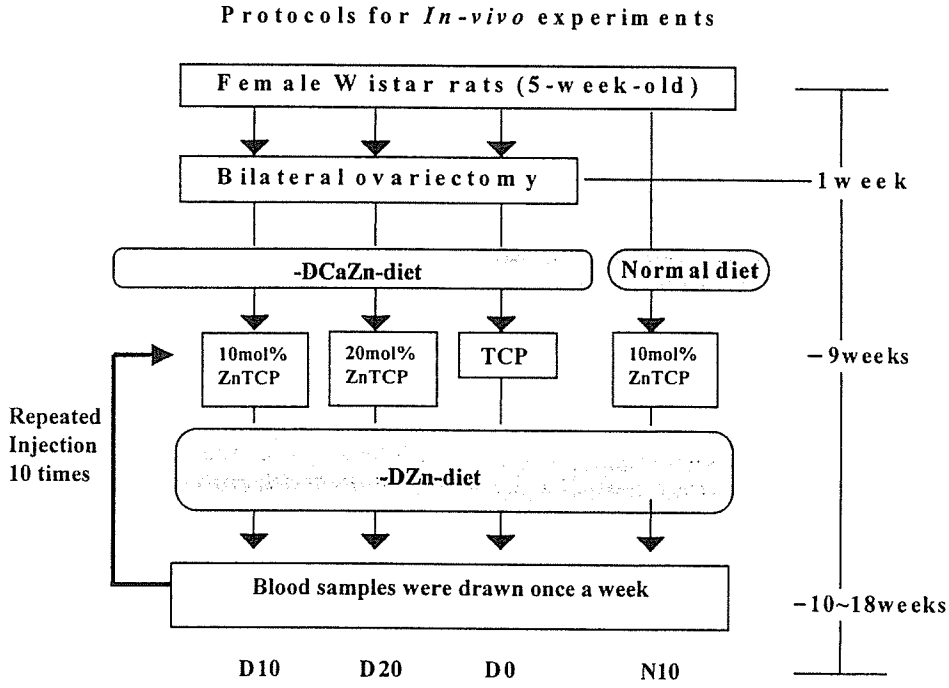

Figure 1. Animal experimental protocols.

times in 9 weeks. The rats in D0, D10, D20, and N10 groups were fed the −DZn-diet for the second 9 weeks to recover from the osteoporosis, as shown in Figure 1. Blood samples were obtained at predetermined time intervals from the tail vein.

Plasma alkaline phosphatase activity measurements

Plasma alkaline phosphatase (ALP) activity was determined by the phenyl phosphoric acid method[14] using commercially available measurement kits (Wako Chem., Co., Japan) and a UV-visible spectrometer (Type UV160. Shimadzu Co. Ind., Japan). All data are expressed as average values ± standard deviation of four different measured values. The area under the curve of plasma ALP level (ALP-AUC) was calculated by integration of the plasma ALP level profile as a parameter.

Bone mineral density (BMD) measurement

Both diseased and healthy rats were anesthetized by ether inhalation. BMDs of the lumbar vertebra and femurs of the anesthetized rats were determined by based on the transmission of soft X-rays using a bone mineral densitometer (model DCS-600R, Aroka Co., Japan). All data were expressed as average values ± standard deviation of four different measured values. The lumber vertebra BMD of the rats independently housed for 9 week under the same condition as the D0, D10 ,and D20 groups was 55.2 ± 4.8 mg/cm^2 (n = 4), but that of the normal rat under the same as the N group was 112.3 ± 11.0 mg/cm^2 (n = 4); this result indicated that the rats in the D0, D10, and D20 groups were induce osteoporosis by feeding of −DCaZn-diet after the first 9 weeks.

Statistical test

Student's t-test was used to determine significant differences between two independent groups. One-way analysis of variance test (ANOVA) was used to determine significant differences among four groups.

RESULTS

Effect of Zn–TCP injections on plasma Zn level in diseased rats

Injection of the Zn–TCP powder suspension led to the recovery of plasma Zn levels in diseased rats (Fig. 2). Average plasma Zn level of normal, healthy rats was about 2 μg/mL, as indicated by the plasma Zn level in the N10 group before Zn–TCP injection. However, plasma Zn levels in the diseased rats in the D0, D10, and D20 groups, were about 1.5 μg/mL before the injections. The plasma Zn level in the D20 group increased gradually after the first injection, and reached 2.7 μg/mL on the day of the second injection (day 7). Plasma Zn levels in the D10 group started to increase after the third injection on day 14. The plasma

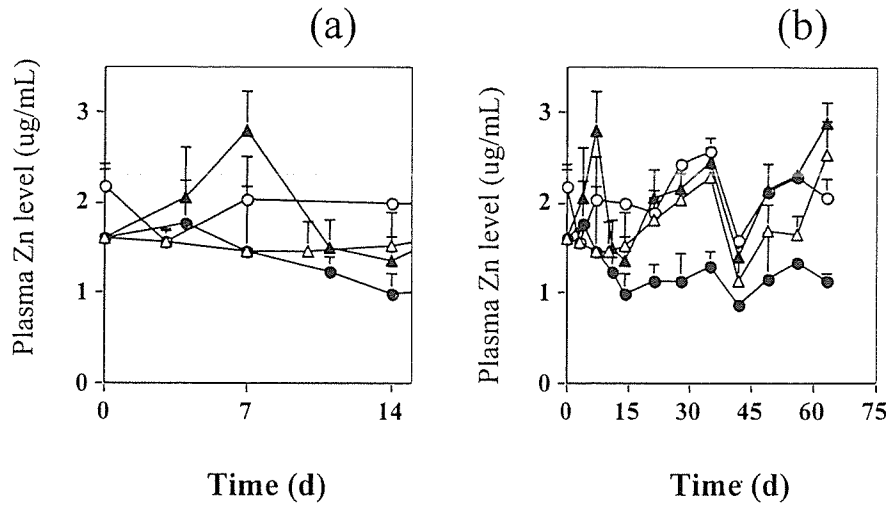

Figure 2. Plasma Zn levels in healthy and diseased rats after ZnTCP suspension injections. (a) Initial stage, (b) whole experimental period. △, D10 group; ▲, D20 group; ●, D0 group; ○, N10 group. The symbols and bars represent the average and standard deviation (n = 4), respectively.

Zn levels of the rats receiving Zn containing injections (D10, D20, and N10) began to rise after day 14 and remained elevated from then until the end of the experiments on day 63. During this period, the plasma Zn levels for these animals rose to the 2.7 μg/mL, fell to about 1.5 μg/mL and then rose again toward the end of the test period. In contrast, the rats that received injections containing no Zn showed plasma Zn levels that remained nearly constant at 1.0 ± 0.2 μg/mL from day 14 on.

There was no significant difference in the Zn-AUC between the N10 and D20 goups, indicating a therapeutic effect of Zn–TCP injection on the recovery of plasma zinc levels (Fig. 3). The overall order of Zn-AUC was N10 ≅ D20 > D10 > D0. Zn-AUCs for the D10 and D0 groups were significantly lower than those of the group N10 and D20 groups ($p < 0.05$).

Effect of Zn–TCP injection on plasma calcium level in diseased rats

Plasma calcium levels in all diseased group models increased to a normal level following the calcium-supplemented feeding diet as well as injection of the calcium-containing suspension (Fig. 4). The average plasma calcium level for healthy rats was 11.0 ± 1.2 mg/dL, as indicated by plasma calcium levels of the N10 group before the injection experiment. However, the average plasma calcium levels in diseased rats was about 6 mg/dL before the injection experiment, and were significantly lower than in the N10 group. After starting the injections and adding calcium content to the diet, the plasma calcium levels in all diseased groups increased to the normal calcium level. This suggested that the D0 group animals attained normal plasma calcium level without Zn administration. The Ca-AUC for the N10 group was significantly higher than any of the D0, D10, and D20 groups (Fig. 5). There was no significant difference in the Ca-AUCs among the D0, D10, and D20 groups.

Effect of Zn–TCP injection on ALP activity in diseased rats

Injection of the Zn–TCP powder suspension led to an increase in ALP activity in diseased rats (Figs. 6 and

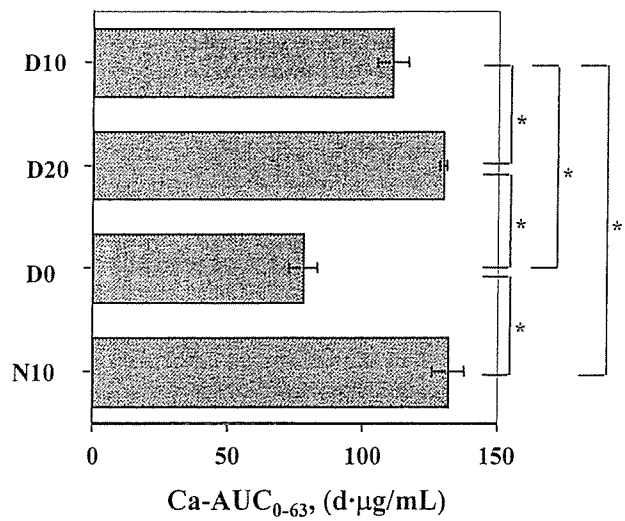

Figure 3. The area under the curves of plasma Zn (Zn-AUC) for healthy and diseased model rats after ZnTCP suspension injections. All data are expressed as the average of four different measured values ± standard deviation. *, Student's t-test was used to determine the significance of differences in level, and a p-value of 0.05 was considered significant.

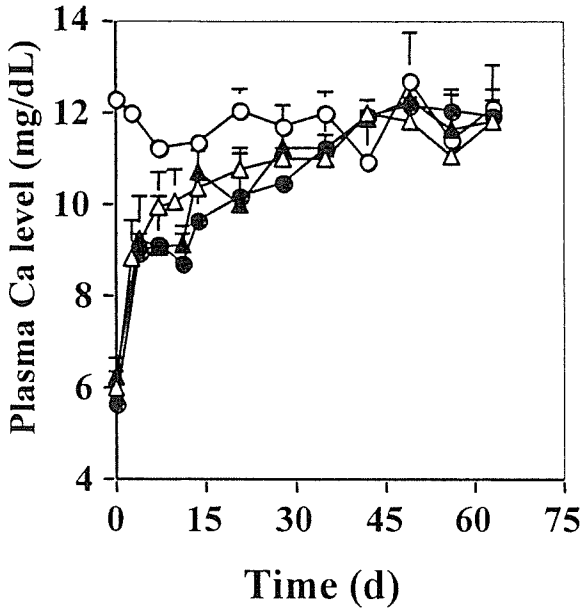

Figure 4. Plasma Ca levels of healthy and diseased rats after ZnTCP suspension injections. △, D10 group; ▲, D20 group; ●, D0 group; ○, N10 group. The symbols and bars represent the average and standard deviation (n = 4), respectively.

7). ALP activity in all groups decreased in the initial stage from 0 to 7 days, and gradually increased and reached the maximum level on day 35, and then rapidly decreased on day 42. During this change, the ALP activity in the D10 and D20 groups was maintained at a level higher than that in the N10 group.

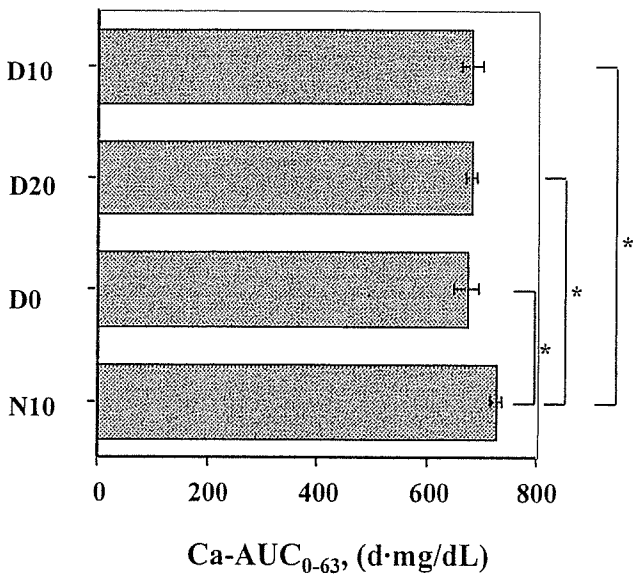

Figure 5. The area under the curves of plasma Ca (Ca-AUC) for healthy and diseased rats after ZnTCP suspension injections. All data are expressed as the average of four different measured values ± standard deviation. *, Student's t-test was used to determine the significance of differences level, and a p-value of 0.05 was considered significant.

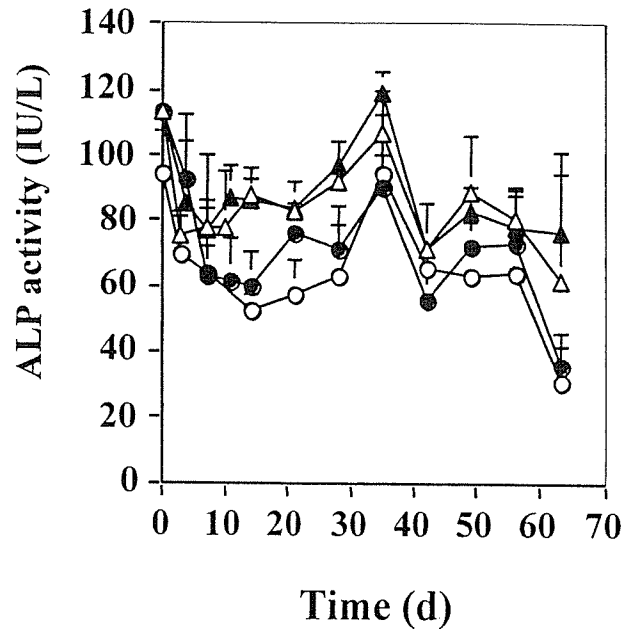

Figure 6. Plasma alkaline phosphatase (ALP) activity profiles for healthy and diseased rats after ZnTCP suspension injections.△, D10 group; ▲, D20 group; ●, D0 group; ○, N10 group. The symbols and bars represent the average and standard deviation (n = 4), respectively.

The ALP activity during the entire experimental period was on the order of N10 < D0 &l;t D10 = D20, which was shown by the ALP-AUC (Fig.7). The ALP-AUCs for the D10 and D20 groups were nearly equivalent, but were significantly higher than those for the D0 and N10 groups (p < 0.005). The results suggest

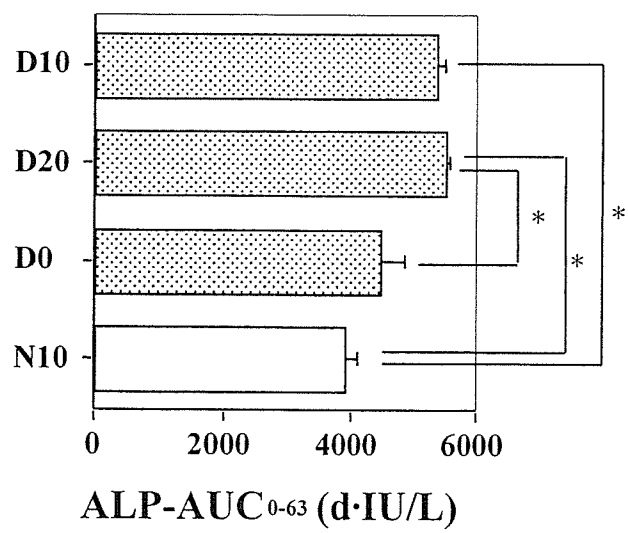

Figure 7. The area under the curves of plasma ALP (ALP-AUC) for healthy and diseased rats after ZnTCP suspension injections. All data are the average of four different measured values ± standard deviation. *, Student's t-test was used to determine the significance of difference in level, and a p-value of 0.05 was considered significant.

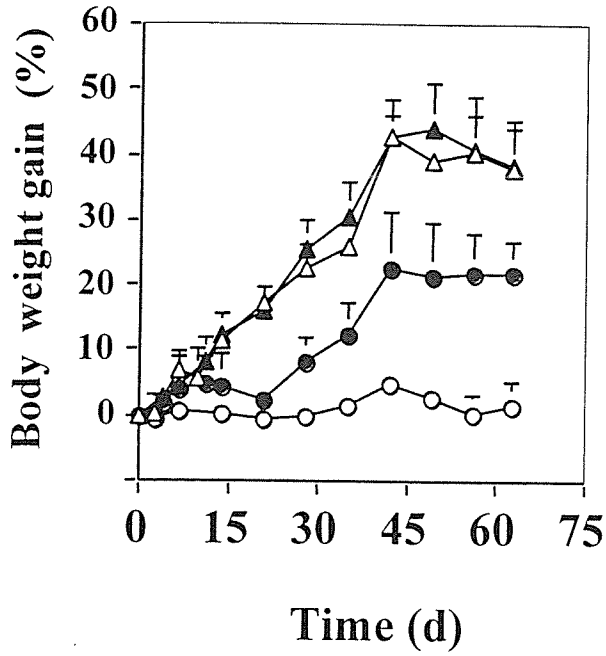

Figure 8. Effect of ZnTCP suspension injections on body weight gain of healthy and diseased rats. △, D10 group; ▲, D20 group; ●, D0 group; ○, N10 group. The symbols and bars represent the average and standard deviation (n = 4), respectively.

that Zn–TCP suspension injection had a stimulatory effect on cell activity in the diseased rats.

Effect of Zn–TCP injection on body weights of diseased rats

Body weights of rats in the D10 and D20 groups increased significantly immediately after starting the injections (Fig. 8), and reached a constant value of about a 45% gain at day 45. The body weights of rats in the D0 group started to increase after day 21, and reached a constant value of about a 20% gain at day 45. The increase for the D0 group might be due to calcium supplements. The increases in the body weights of the D10 and D20 groups were significantly higher than that of the D0 group, and although the plasma calcium concentration of the D0 group was rising to a normal calcium level, the weight of a rat did not increase. In contrast, the body weight of rats in the N10 group remained unchanged during the entire period of injections because the rats had reach maturity and had already attained a constant body weight before the injections were started.

Relationship between body weight and cumulative Ca-AUC or Zn-AUC in diseased rats

Cumulative calcium area under the curve (Ca-AUC) was calculated from plasma calcium levels in Figure 4. Figure 9 shows the relationship between the increase in body weight and the cumulative Ca-AUC. The body weights of the D10 and D20 groups increased significantly with increasing Ca-AUC, and reached nearly a constant value of about 40%. Similarly, the D0 group increased to about 20%. In contrast, the body weight of the N10 group was not raised to depend on the Ca-AUC.

Figure 10 shows the relationship between increase in body weight and cumulative Zn-AUC. The body weight gains of the D0, D10, and D20 groups were all approximately proportional to the average plasma Zn levels, but the slopes of the D10 and D20 groups were slightly higher than that of the D0 group. The body weight of the N10 group did not increase.

Effect of Zn–TCP injection on bone mineral density in diseased rats

Zn–TCP suspension injection resulted in a local increase in bone mineral density (BMD), that is, in the vicinity of the injection site (Fig. 11). All the injections were administered intramuscularly in the left thigh. The BMD of the left femur was significantly higher than that of the right in both the D10 and D20 groups on day 63 (Student t-test; $p < 0.05$). However, there was no significant difference in the BMD between the left and right femur in the D0 and N10 groups. The BMDs of the left femur of the D10 and D20 groups

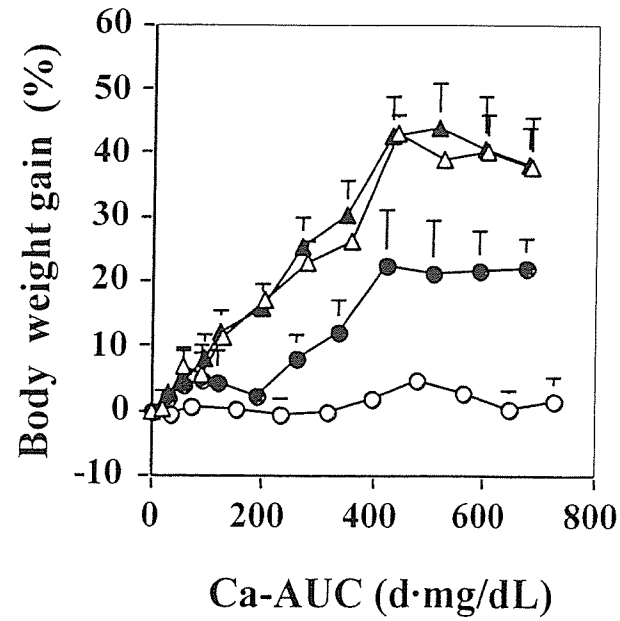

Figure 9. Effect of The area under the curves of plasma Ca (Ca-AUC) on increase in body weight of healthy and diseased rats after ZnTCP suspension injections. △, D10 group; ▲, D20 group; ●, D0 group; ○, N10 group. The symbols and bars represent the average and standard deviation (n = 4), respectively.

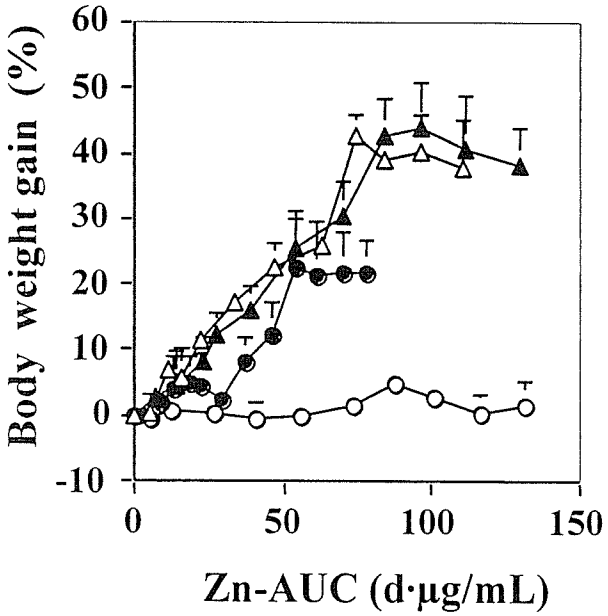

Figure 10. Effect of the area under the curves of plasma Zn (Zn-AUC) on increase in body weight of healthy and diseased rats after ZnTCP suspension injections. △, D10 group; ▲, D20 group; ●, D0 group; ○, N10 group. The symbols and bars represent the average and standard deviation (n = 4), respectively.

were significantly higher than that of the D0 group. The overall the rank order of the BMD of the femurs was D0R ≤ D0L < D10R ≤t D20R < D10L < D20L. There was no significant difference in femur BMD between the D20L and N10 groups, and between the

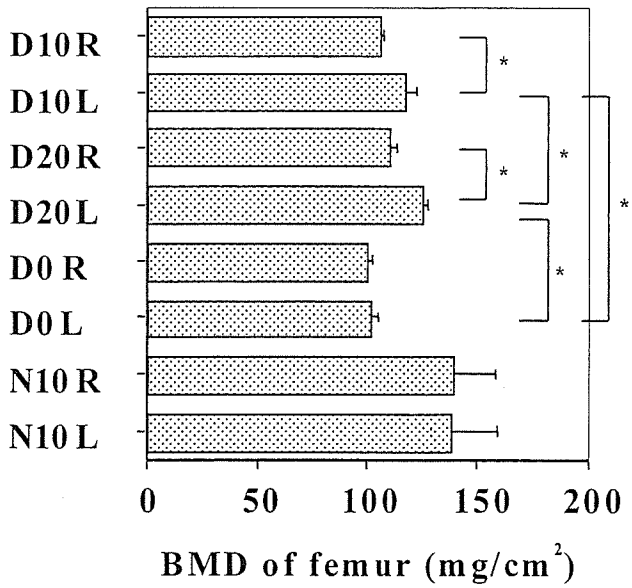

Figure 11. Effect of ZnTCP suspension injections on bone mineral density (BMD) of femur of healthy and diseased model rats. All data are the average of four different measured values ± standard deviation. *, Student's t-test was used to determine the significance of differences in level and a p-value of 0.05 was considered significant.

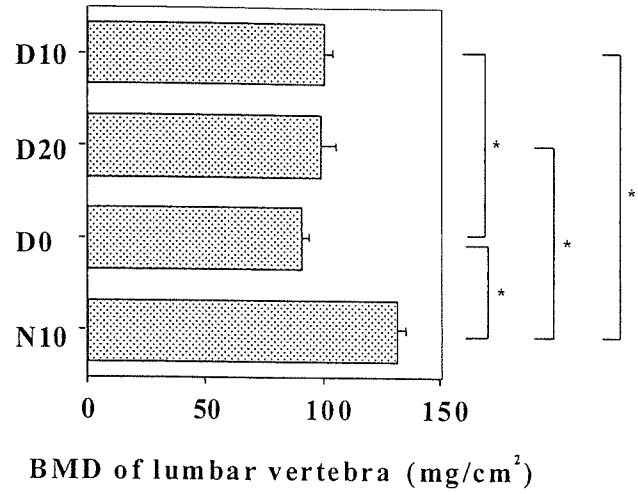

Figure 12. Effect of ZnTCP suspension injections on bone mineral density (BMD) of lumbar vertebra of healthy and diseased rats. All data are the average of four different measured values ± standard deviation. *, Student's t-test was used to determine the significance of differences in level and a p-value of 0.05 was considered significant.

D10R and N10 groups. On the other hand, BMD of the lumbar vertebra of the D10 and D20 groups was significantly lower than that of the N10 group on day 63, as shown in Figure 12 (ANOVA; $p < 0.005$). Figure 13 shows the soft tissue in the vicinity of the left thigh of a rat from the D10 group on day 63. No inflammation or ZnTCP particles were noted in the injected site by macroscopic observation.

DISCUSSION

Effect of Zn–TCP suspension injection on plasma Zn, Ca, and ALP levels in diseased rats

In the present study, 20 mol % Zn–TCP injection was more effective than 10 mol % Zn–TCP in increasing the plasma Zn and ALP levels, and consequently BMD. The first 20 mol % Zn–TCP injections induced a rapid increase in plasma Zn level in diseased rats. However, two injections were necessary in the case of the 10 mol % Zn–TCP injections to increase the plasma Zn level. In both cases, 2.7 μg/mL was the maximum plasma Zn level reached. Once the plasma Zn reached 2.7 μg/mL, it always decreased to 1.5 μg/mL. ALP activity also exhibited a periodical change similar to the plasma Zn level. Because high plasma Zn levels are cytotoxic,[1] it may be that these Zn levels are regulated physiologically as a homeostatic reaction. In the body, there are metallothioneins that function as a storage system for heavy metals. Metallothioneins may be involved in the regulation of plasma Zn levels because excessive Zn levels cause cell toxicity.[1]

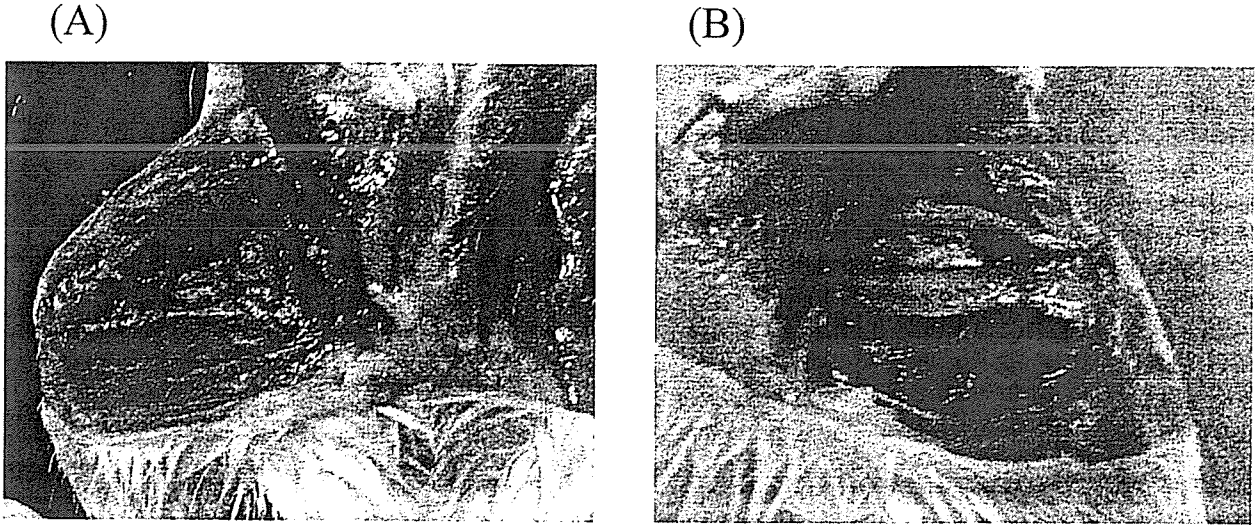

Figure 13. Photographs of soft tissue of the D1 group after on day 63. (A) Right leg (control), (B) left leg (ZnTCP-injected site).

Effect of Zn–TCP injection on body weight of diseased rats and relationship between body weight and cumulative Ca-AUC or Zn-AUC

Differences in increase in body weight between the D10 and D0 groups, or between the D20 and D0 groups can be attributed to the pharmacological effect of Zn released from Zn–TCP. Because weights of bones and muscles account for approximately 20 and 50% of the total body weight, respectively, body weight is a parameter that reflects bone generation. The body weight of the D10 and D20 groups increased significantly compared to the D0 group during the entire experimental period (Fig. 8). The increase in the body weight of the D0 group may only be due to calcium intake from the diet and TCP in the suspension. The body weight of the N10 group remained unchanged during the entire experimental period because these were fully mature animals and had already attained a constant body weight. Therefore, it appeared that the differences between the D10 and D0 groups, or between the D20 and D0 groups, were actually due to the pharmacological effects of Zn rather than to the disease itself.

In the relationship between the body weight and cumulative Ca-AUC (Fig. 9), the body weights of the D10 and D20 groups increased significantly with increasing Ca-AUC. In contrast, the D0 group had the lowest plasma Zn level, and the body weight only increased by about 20%. It may be that cell activity related to increased body weight was not induced. These results suggest that the combination of Ca and Zn supplementation is important for growth improvement of diseased rats. These results also suggest that the low body weight gain of the D0 group compared to that of the D10 and D20 groups might be due to the pharmacological effect associated with Zn release. The results further indicate that a sufficient plasma Ca level in the diseased rats is necessary for body growth. In addition, a suitable plasma Zn level supplied by the Zn–TCP injection, may affect the Ca that is available for increasing body weight. On the other hand, Zn–TCP injections did not affect the body weight of the N10 group, because the N10 group was mature and had attained a constant body weight prior to initiation of the experiment. In the relationship between body weight and cumulative Zn-AUC (Fig. 10), the body weight gains of the D0, D10, and D20 groups were proportional to average plasma Zn levels. These results suggest that the increase in body weight of diseased rats was proportional to the cumulative plasma Zn level. It also appears that the plasma Zn level in the D0 group was only sufficiently high enough to induce a low body weight gain. This suggests that lower Zn levels inactivate enzymes essential for growth.[1]

Effect of Zn–TCP injection on BMD of diseased rats

Zn–TCP injection appears to be pharmacologically effective in correcting bone mineral deficiency with its local effect being more pronounced than its systemic effect. BMD of vertebral bones is known to reflect the balance between absorption and deposition of bone minerals in the whole body. Therefore, the BMD of vertebral bones was used as an indicator of whole-body effect of Zn–TCP on BMD of the diseased rats. The BMD of the vertebral bones of the D10 group was significantly higher than that of the D0 group, although that of the D20 group is not significant, as